

Spin alignment and phase angles in $^{12}\text{C} + ^{12}\text{C}$ inelastic scattering

S. J. Willett,* S. K. Korotky,† R. L. Phillips,‡ and D. A. Bromley

Wright Nuclear Structure Laboratory, Yale University, New Haven, Connecticut 06511

K. A. Erb§

Wright Nuclear Structure Laboratory, Yale University, New Haven, Connecticut 06511
and Oak Ridge National Laboratory, Oak Ridge, Tennessee 37830

(Received 19 January 1983)

The spin alignment A and the relative phase angle β between the $m = +2$ and -2 substates populated in $^{12}\text{C} + ^{12}\text{C}(2_1^+)$ inelastic scattering were measured over a wide range of particle scattering angles ($53^\circ < \theta_{\text{c.m.}} < 101^\circ$) and interaction energies ($15 < E_{\text{c.m.}} < 33$ MeV). Although the substate population parameters depend rather strongly on reaction angle, the angle-averaged alignment is markedly enhanced at energies where either broad or narrow maxima occur in $\sigma(E)$, at least below $E_{\text{c.m.}} = 26$ MeV. Above that energy variations in the alignment become damped with respect to both bombarding energy and reaction angle. The relative phase $\beta(\theta)$ is approximately linear in θ at most energies. For energies below $E_{\text{c.m.}} = 26$ MeV corresponding to gross structure maxima in the inelastic cross sections, the measured dependence of the phase on reaction angle suggests that the reaction is dominated at these energies by individual entrance and exit channel partial waves L and L' , respectively, and that these are related by $L' = L - 2$. Thus a strongly aligned configuration can be associated with the maxima. At neighboring energies no evidence for such alignment was found. Calculations with the band-crossing, diffraction, distorted-wave Born approximation, and barrier-top models were compared to the measurements. None provide an adequate representation of the data.

[NUCLEAR REACTIONS $^{12}\text{C}(^{12}\text{C}, ^{12}\text{C}\gamma)$, $E_{\text{lab}} = 30\text{--}65$ MeV, $\theta_{\text{c.m.}}(^{12}\text{C}) = 53^\circ\text{--}101^\circ$. Measured particle- γ angular correlations; deduced magnetic substate alignments, phase angles; compared with model predictions.]

I. INTRODUCTION

The discovery by Cormier *et al.*^{1,2} of prominent gross structure in the excitation function of $^{12}\text{C} + ^{12}\text{C}$ inelastic scattering has rekindled interest in determining the physical processes that underlie the gross structure phenomenon. Cormier *et al.* initially suggested that the broad maxima observed above the Coulomb barrier, characteristically a few MeV in width, reflect single-particle resonance states in the relative motion of the two carbon nuclei. Subsequent theoretical treatments involving variations of the double resonance model,³ carried out, for example, by Konnecke *et al.*,⁴ Kondo *et al.*,⁵ and Tanimura⁶ successfully reproduced the gross features of the elastic and inelastic yields and provided a general framework for the interpretation of the cross section data.

However, an angular correlation experiment⁷ indicated that the broad structures were not characterized by a unique spin, in contradiction to the assumptions of the theoretical resonance models, while other researchers have found the data to be consistent with other mechanisms. Phillips *et al.*⁸ have reproduced the structures with a diffraction model. Cannell *et al.*⁷ found that an adjustment in the optical potential of Reilly *et al.*⁹ would produce gross structures at the desired energies from a distorted-wave Born approximation (DWBA) calculation. Lee

*et al.*¹⁰ have proposed that the structure arises from interference between interior and surface-reflected waves, while Friedman *et al.*¹¹ have characterized the data as evidence for barrier-top resonances.

The discovery by Paul *et al.*,¹² that a correlated excitation function gross structure also appears in $^{16}\text{O} + ^{16}\text{O}$ inelastic yields for channels which are poorly matched in angular momentum to the entrance channel, presented a severe test for resonance and nonresonance models alike. Only the strong coupling calculations recently reported by Tanimura and Mosel¹³ describe these data successfully. In contrast to the other calculations mentioned above, which rely essentially on the angular momentum matching between entrance and exit channel optical model wave functions and which, therefore, lead to incorrect predictions for the poorly matched channels studied by Paul *et al.*, the strong coupling employed in Ref. 13 induces large shifts in the wave-function-equivalent local potentials to achieve good angular momentum matching even in these channels.

Thus, while angular momentum matching remains the key ingredient in current descriptions of the inelastic yields, the matching may be achieved with a variety of distinctly different mechanisms. Additional information concerning the role of these mechanisms may be gained from measurements of the magnetic substate population

parameters for nuclear states excited in the inelastic processes. As initially noted in Refs. 5 and 8, and discussed in detail by Tanimura and Mosel,¹⁴ the matching conditions inherent in the more successful theoretical models lead to a characteristic alignment of the excited nucleus along an axis perpendicular to the reaction plane. This alignment can be probed directly through measurements of the gamma-decay intensity in coincidence with the scattered projectiles. In the specific case studied in the present work— $^{12}\text{C} + ^{12}\text{C}$ inelastic scattering involving the 4.43 MeV 2_1^+ level—choosing a quantization axis normal to the reaction plane, only the ratio of the intensities associated with the $|m|=2$ and $m=0$ substates need be measured to test the alignment hypothesis. However, additional valuable information accrues from measurement of the complete in-plane angular correlation, in that phases as well as magnitudes of the 2_1^+ wave function components can be determined. As shown below, the dependence on reaction angle of the relative phase β between the $m=+2$ and $m=-2$ substates provides a sensitive measure of the extent to which nonaligned configurations and more than one entrance channel partial wave participate in the production of the excitation function gross structure.

Angular correlations between inelastically scattered ^{12}C nuclei ($Q = -4.44$ MeV) and the corresponding gamma-decay radiation were measured at 19 energies between $E_{\text{c.m.}} = 15.6$ and 32.4 MeV. The energies were chosen to map over both broad and intermediate width structures observed in the inelastic scattering differential and total cross sections. Complete in-plane correlation patterns

were measured at each energy for closely spaced reaction angles throughout the range $53^\circ \leq \theta_{\text{c.m.}} \leq 101^\circ$. Magnetic substate population parameters were extracted from these data for a total of 333 bombarding-energy—reaction-angle pairs. Preliminary reports of portions of these data have appeared previously.^{15,16} The present paper augments these brief reports of the alignment measurements with new information concerning the substate phases, detailed measurement of the absolute magnitudes of the correlation functions, and comparisons of various model predictions with the data.

Studies of spin alignment for the reaction considered here have also been reported by the Munich group.^{17,18} In that work the emphasis was on detailed excitation function measurements of the alignment for selected reaction angles, whereas the thrust of the present work was to measure detailed angular distributions of both the alignment and substate phase at representative bombarding energies.

II. FORMALISM

Our approach is similar to that used by Hayward and Schmidt.¹⁹ We define the spin quantization axis \hat{z} to be perpendicular to the reaction plane. In this coordinate system, the Bohr theorem²⁰ implies that the only substates allowed for the $J^\pi = 2^+$ excited residual nucleus are $m = -2, 0,$ and $+2$. If the γ radiation emitted in the $E2$ transition to the ground state is observed in coincidence with the ejectile, then the correlation function is the following²¹:

$$W(\psi, \phi) = \frac{5}{16\pi} \sin^2 \psi \{ \alpha_+^2 + \alpha_-^2 + (1 + 5\alpha_0^2) \cos^2 \psi - 2\sqrt{6} \cos^2 \psi [\alpha_+ \alpha_0 \cos(2\phi + \beta_+ - \beta_0) + \alpha_0 \alpha_- \cos(2\phi + \beta_0 - \beta_-)] - 2\alpha_+ \alpha_- \sin^2 \psi \cos(4\phi + \beta_+ - \beta_-) \}, \quad (1)$$

in the case that the photon's circular polarization is not observed. ψ and ϕ are the polar and azimuthal angles of the photon emission with respect to the quantization axis defined above. α_m and β_m are the amplitude and phase for the population of substate m , with $+$ ($-$) denoting $+2$ (-2). The quantities α_m and β_m are real functions of energy E and particle scattering angle θ .

If the photon is detected in the reaction plane, (1) reduces to

$$W(90^\circ, \phi) = \frac{5}{16\pi} [\alpha_+^2 + \alpha_-^2 - 2\alpha_+ \alpha_- \cos(4\phi + \beta_+ - \beta_-)]. \quad (2)$$

No $m=0$ radiation occurs in the reaction plane, but we can deduce α_0 from the unitarity condition

$$\sum_m (\alpha_m)^2 = \alpha_+^2 + \alpha_-^2 + \alpha_0^2 = 1.$$

Techniques used to deduce the absolute normalization of the correlation function are discussed in the next section.

The experiment did not distinguish which of the two carbon ions emerging from the reaction had been excited. However, since the particles in the entrance channel are identical, it can be demonstrated²¹ that the correlation function $W(\psi, \phi)$ is the same in either case. The two cases correspond to antiparallel definitions of the quantization axis; however, Eq. (1) is symmetric with respect to $m = +2$ and -2 . Alignment is defined as the probability of populating *either* the $m = +2$ or -2 substate: $A = \alpha_+^2 + \alpha_-^2$. As long as we choose to measure the alignment, and not the polarization, distinction of the two exiting carbon ions need not concern us. The very small difference in the laboratory to center-of-mass transformations is negligible.

The experimental angular correlations are fitted, not with the function of Eq. (1), but rather with a function W' that takes the finite solid angles of the detectors into account. Our gamma detectors subtended a much larger solid angle than the particle detector, so corrections for the latter are neglected. We define the measured correlation function as

$$W'(\psi, \phi) = \frac{\int_{\phi-\delta\phi}^{\phi+\delta\phi} d\phi \int_{\psi-\delta\psi}^{\psi+\delta\psi} W(\psi, \phi) \sin\psi d\psi}{\int_{\phi-\delta\phi}^{\phi+\delta\phi} d\phi \int_{\psi-\delta\psi}^{\psi+\delta\psi} \sin\psi d\psi}, \quad (3)$$

where $\delta\psi$ and $\delta\phi$ are the effective half angles of the photon detectors, which are NaI scintillators. The $\delta\psi$ and $\delta\phi$ are estimated from the geometry by replacing the circular cross section of the NaI crystal halfway through its depth by a square of equal area, and assuming that the detector response function is flat over that solid angle. Letting $x = \cos\psi$, Eqs. (1) and (3) imply

$$W'(\psi, \phi) = c_0 + c_1 Q_2 x^2 + c_2 Q_4 x^4 + K_2 (Q_2 x^2 - Q_4 x^4) (c_3 \cos 2\phi + c_4 \sin 2\phi) + K_4 (1 - 2Q_2 x^2 + Q_4 x^4) \times (c_5 \cos 4\phi + c_6 \sin 4\phi), \quad (4)$$

where

$$\begin{aligned} Q_2 &= \cos^2 \delta\psi + \frac{1}{3} \tan^2 \psi \sin^2 \delta\psi, \\ Q_4 &= \cos^4 \delta\psi + 2 \tan^2 \psi \cos^2 \delta\psi \sin^2 \delta\psi + \frac{1}{5} \tan^4 \psi \sin^4 \delta\psi, \\ K_2 &= \frac{\sin 2\delta\phi}{2\delta\phi}, \quad K_4 = \frac{\sin 4\delta\phi}{4\delta\phi}, \\ c_0 &= \frac{1}{4\pi} [1 - \alpha_0^2 + \frac{1}{4} (\alpha_+^2 + \alpha_-^2)] \\ &= \frac{5}{16\pi} (\alpha_+^2 + \alpha_-^2) \text{ with proper normalization,} \\ c_1 &= \frac{15}{8\pi} \alpha_0^2, \quad c_2 = -\frac{5}{8\pi} [\frac{1}{2} (\alpha_+^2 + \alpha_-^2) + 3\alpha_0^2], \\ c_3 &= \frac{-5\sqrt{6}}{8\pi} [\alpha_+ \alpha_0 \cos(\beta_+ - \beta_0) + \alpha_0 \alpha_- \cos(\beta_0 - \beta_-)], \\ c_4 &= \frac{5\sqrt{6}}{8\pi} [\alpha_+ \alpha_0 \sin(\beta_+ - \beta_0) + \alpha_0 \alpha_- \sin(\beta_0 - \beta_-)], \\ c_5 &= \frac{-5}{8\pi} \alpha_+ \alpha_- \cos(\beta_+ - \beta_-), \\ c_6 &= \frac{5}{8\pi} \alpha_+ \alpha_- \sin(\beta_+ - \beta_-). \end{aligned} \quad (5)$$

In the reaction plane

$$W'(90^\circ, \phi) = c_0 + K_4 (1 - 2Q_2 x^2 + Q_4 x^4) \times (c_5 \cos 4\phi + c_6 \sin 4\phi), \quad (6)$$

and coefficients from (6) give the parameters of interest:

$$\begin{aligned} \beta &= \beta_+ - \beta_- = \tan^{-1}(-c_6/c_5), \\ A &= \alpha_+^2 + \alpha_-^2 = \frac{16\pi}{5} c_0. \end{aligned} \quad (7)$$

III. EXPERIMENT

The particle-gamma correlation experiments were performed with the Yale MP accelerator, and with natural carbon targets of nominal areal density $100 \mu\text{g}/\text{cm}^2$. As depicted in Fig. 1, the particles were detected by a solid

state position sensitive detector (PSD1), in front of which was placed a thin brass mask with 18 slits of width $\approx 0.7^\circ$ (lab) defining discrete scattering angles θ . For a subset of the energies measured ($E_{\text{c.m.}} > 21.5 \text{ MeV}$), a second PSD was positioned to capture recoil nuclei from the reaction; its purpose is discussed later in this section. Photons were detected in either of two $12.7 \times 12.7 \text{ cm}$ cylindrical NaI(Tl) scintillators placed at angles ϕ_F, ϕ_B with respect to the beam direction and in the reaction plane ($\psi = 90^\circ$). Effective half angles $\delta\psi$ and $\delta\phi$ for the various runs were $10^\circ - 12^\circ$. After amplification, shaping, and timing, on-line analysis of the signals was accomplished using the Yale data acquisition system in conjunction either with an IBM 360-44 (early data) or IBM-4341 (later data) computer.

Particles in PSD1 and gamma radiation from either NaI crystal were analyzed in fast coincidence. Timing resolution was $\sim 30 \text{ ns}$ over the entire length of PSD1, and $\sim 10 \text{ ns}$ for any one particular slit. A software gate defined the region in time vs θ space for true coincidences; random coincidences were subtracted by translation in time of this gate. Further processing of these data consisted of choosing $^{12}\text{C} + ^{12}\text{C}^*(4.439 \text{ MeV})$ events via E vs θ analysis, separating the data into specific slits, and accepting only a fraction of the photon spectrum. That fraction consisted of the photo and escape peaks of 4.439 MeV radiation, with the background from Compton scattering of 6.13 MeV photons (from $^{16}\text{O}^*$) subtracted.

The singles yield (for $E > 21.5 \text{ MeV}$) was determined by kinematic coincidence of particles in the two PSD's (method I). This technique facilitated clean separation of final states consisting of two carbon nuclei from the background, whereupon inelastic scattering could be selected and yields obtained for each slit. For energies $E < 21.5 \text{ MeV}$, PSD2 was not generally used (method II), but we found by direct comparison of the two techniques at three widely-spaced energies that, while use of the particle-particle coincidence method generally was not essential, the singles data at the largest particle angles required background subtraction. As a consequence, alignment magnitudes for $\theta_{\text{c.m.}} > 93^\circ$ may be unreliable and thus are not reported here. The information obtained for the relative phases of the magnetic substate population is not affected by this problem, however.

The experimental correlation function W is simply the ratio of the coincidence to the singles yields, as obtained above, multiplied by an overall normalization constant N . (The singles yield must be divided by 2 because of identical particle symmetry.) N is a function only of the efficiency and solid angle of the gamma detector; its determination is discussed at the end of this section. The data $W(90^\circ, \phi)$ —at least six points—for each E and θ were fitted by a least-squares algorithm to Eq. (6), and the coefficients obtained were converted to the quantities of interest. A typical correlation function and its least square fit are illustrated in Fig. 2.

Because W is the ratio of the coincidence to the singles yields, many corrections applicable to each separately will cancel in the ratio. These include target thickness build-up, equilibrium charge state distribution, integrated beam charge, and electronic dead time. By virtue of the extremely short lifetime of the $^{12}\text{C} 2_1^+$ state, the correction

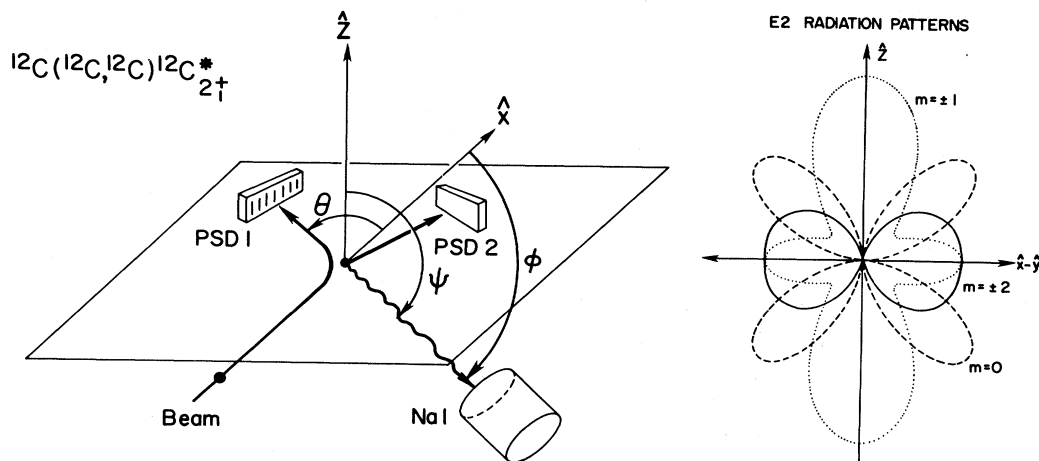


FIG. 1. Left panel: experimental arrangement. Eighteen slits define particle scattering angles θ into a position-sensitive detector PSD1. PSD2 detects recoil particles in kinematic coincidence in method I. γ radiation is detected at angles (ψ, ϕ) with respect to the coordinate axes as shown. Right panel: $E2$ radiation patterns. For our case, the x - y plane is the reaction plane. In this plane the $M = \pm 2$ radiation (solid line) is maximum, while $m = 0$ radiation (dashed line) vanishes. $m = \pm 1$ radiation (dotted line), the only substate classically allowed to have any amplitude in the z direction, is forbidden in the specific nuclear reaction we consider.

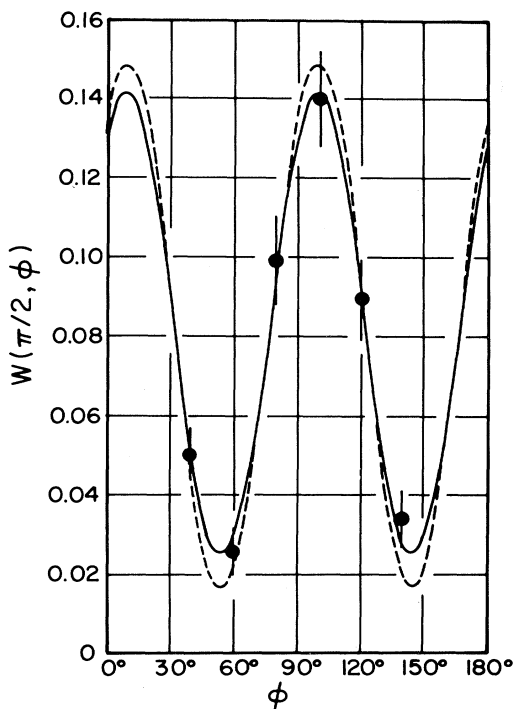


FIG. 2. Typical in-plane correlation function. These data were taken at $E = 17.31$ MeV and $\theta = 78.86^\circ$. The solid curve is a least squares fit to the data incorporating the correction factors K and Q of Eq. (5). To illustrate the effect of finite γ -angular acceptance, the dashed line is generated from the coefficients obtained from the least squares fit, but with the solid angle correction factors neglected.

for the hyperfine interaction is negligible. It was necessary, however, to incorporate a relativistic correction for the motion of the gamma radiation source.

Three methods were employed to determine the absolute normalization constant, N . First, a study of the $^{12}\text{C}(\alpha, \alpha'\gamma)^{12}\text{C}$ reaction was made throughout the angular range $\theta_{\text{c.m.}} = 84^\circ - 122^\circ$, and the results compared to those obtained previously by Hayward *et al.*¹⁹ Phase angles and relative alignments obtained in the two studies were in excellent agreement, and the value $N = 13.42(\pm 8\%)$ was obtained.

A second determination of N was achieved by measuring a "complete" angular correlation of the reaction $^{12}\text{C}(^{12}\text{C}, ^{12}\text{C}'\gamma)^{12}\text{C}$ both in and out of the reaction plane. We used solid state particle telescopes in conjunction with the NaI photon detectors to measure the correlation function at 17 sets of gamma angles (ψ, ϕ) for each of four particle angles θ at $E_{\text{c.m.}} = 29.72$ MeV. The data were fitted with the general form of the correlation function, Eq. (4). Since α_+ , α_- , and α_0 are all measured directly in this experiment, imposition of unitarity $\sum_m (\alpha_m)^2 = 1$ yields the absolute normalization. We found N to be independent of θ , as it must be, and equal to $13.86(\pm 10\%)$.

Third, the technique of Ref. 19 was also used. Angular distributions of protons and photons from the $^{12}\text{C}(p, p')^{12}\text{C}$ reaction were separately measured and integrated, and their comparison yielded $N = 15.70(\pm 12\%)$. This result is approximately one standard deviation higher than the other two, and may be attributed to possible systematic effects that might enter in this singles technique. Therefore, we have adopted the mean of the first two methods— $N = 13.64(\pm 14\%)$ —as the absolute normalization constant.

IV. RESULTS

Figure 3 displays the measured alignments versus angle for the 21 energies measured. Data were taken at approxi-

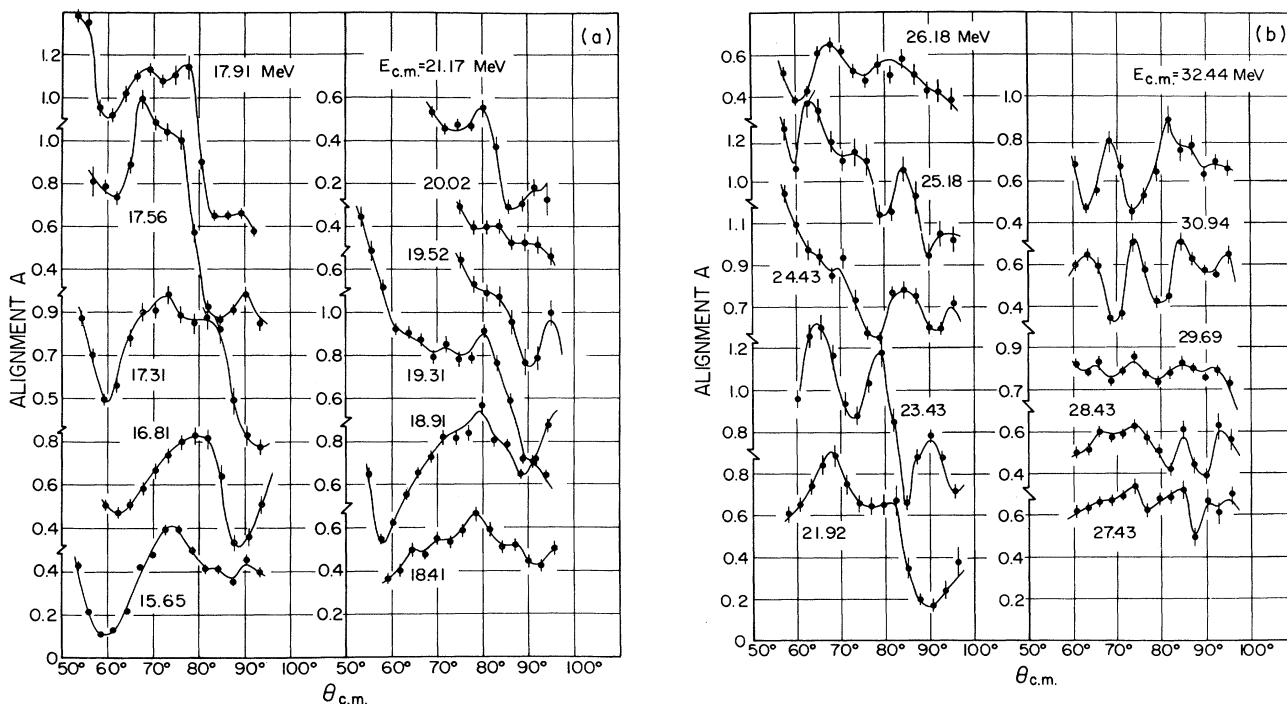


FIG. 3. Alignment versus angle for each energy. The error bars incorporate statistical and other relative errors, but not the absolute normalization uncertainty $\pm 14\%$. The lines are drawn merely to guide the eye.

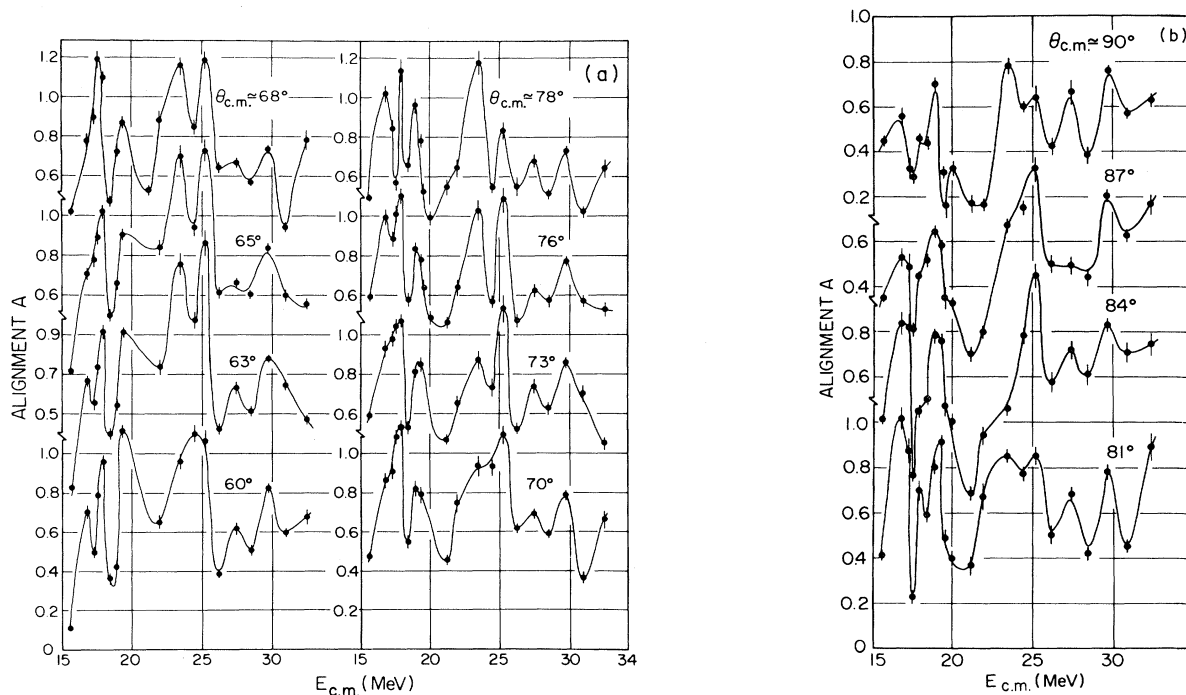


FIG. 4. Alignment versus energy for each angle. The data of Fig. 3 are replotted for the indicated average angles; the angular bins are $2^\circ-3^\circ$ wide. The same comments concerning error bars and solid lines in Fig. 3 apply here.

mately the same angles ($\pm 1.0^\circ$) for each energy, and they are replotted in Fig. 4 to display the energy dependence. In all of these figures, the error bars illustrated encompass only statistical and relative errors; the overall uncertainty of 14% in the absolute normalization is not included. Of the 333 bombarding-energy–reaction-angle pairs for which complete in-plane particle-gamma angular correlations were measured, 11 yielded unphysical results in that the absolute magnitudes of the associated alignments exceeded 1.0 by more than one—but less than two—standard deviations. Despite careful reanalysis of these data, we have been unable to find any instrumental error which might account for this discrepancy, nor have we found any evidence that our data reduction procedures need revision. All the available information supports the internal consistency of our data, raising the possibility that the entire data set should be renormalized (by 20–30%) to avoid the 11 unphysical results. At the present time, data which would justify this otherwise arbitrary step are not available and thus we have chosen to present the alignments as measured. It is important to note in this context that the measured *phases*—which constitute a significant result of the measurements—are independent of this question of overall normalization.

As Fig. 3 illustrates, the alignments deduced from the data depend rather strongly on reaction angle. It is therefore of interest to examine the extent to which the excitation function of the *average* alignment displays any characteristic features. We have averaged the alignment with respect to angle, with the results shown in the center panel of Fig. 5. The center of the shaded region is the mean alignment for $\theta = 59^\circ - 90^\circ$ (except for $19.5 < E_{c.m.} < 21.2$ MeV, where the measured angular range is more restricted), and the width corresponds to ± 1 standard deviation. Thus for each energy, roughly two thirds of the angles measured have A falling within the shaded region. If the 11 alignments with $A > 1$ were renormalized to $A = 1$, the center of the shaded region would change only slightly in Fig. 5, but the vertical width would decrease noticeably.

Also shown in Fig. 5 (bottom panel) is the differential cross section integrated over a comparable angular range. The similarity of the two excitation functions is apparent and remarkable; for $E < 26$ MeV, both broad and narrow maxima in σ are accompanied by enhanced alignments. The deep, broad minimum in the alignment near 20 MeV represents data measured over a somewhat more limited angular range (see Fig. 3), so that the average values are less well determined at $E_{c.m.} = 19.51, 20.02, 21.17$ MeV. But for energies above 26 MeV, the alignment is not as large as might have been expected from a simple extrapolation of the lower energy correlation between A and σ . The narrow width of the shaded band implies that the variation of A with θ is much smaller at these higher energies. These features of the alignment data must be reproduced by any successful model of the inelastic scattering. A comparison of several model calculations with experiment is presented in the next section.

While the origin of broad structures observed in $\sigma(E)$ may be in doubt, the *narrow* peaks undoubtedly reflect genuine resonance behavior. Evidence for this conclusion

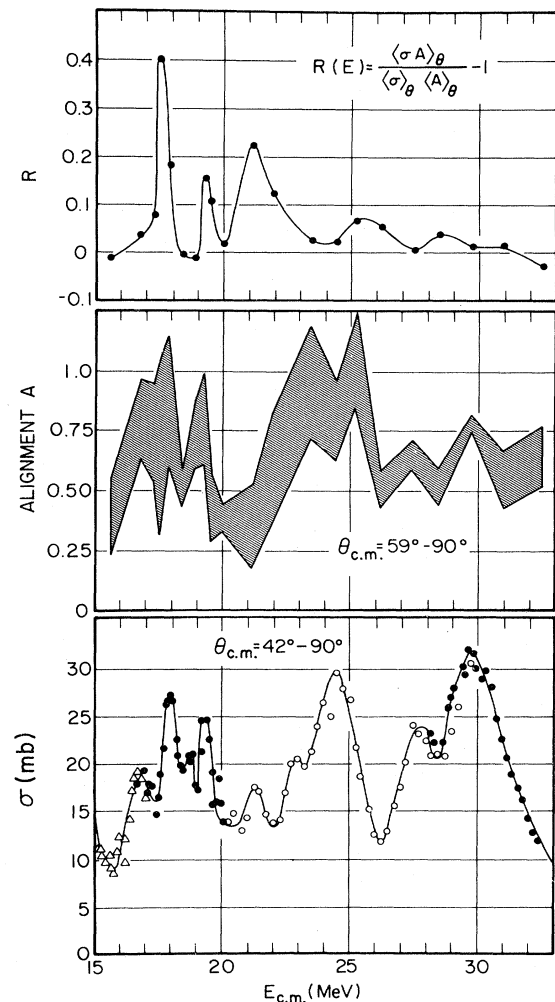


FIG. 5. Top panel: cross correlation between the alignment and differential cross section angular distributions. Center panel: angle-averaged alignment, as described in the text. Bottom panel: angle integrated differential cross section data, from Ref. 17.

accrues partly from the existence of correlated maxima in other exit channels. For example, corresponding to the peak near 17.9 MeV, James and Fletcher²² report a 12^+ resonance at 17.78 MeV from their study of the ^8Be exit channel. Similarly, a maximum near 19.3 MeV has been seen in a number of channels: proton,²³ neutron,²⁴ deuteron,²⁵ ^8Be (12^+ at 19.46),²² and elastic (12^+ at 19.4).²⁶ A complete discussion of correlations among a variety of exit channels may be found in Ref. 27. It is significant that at center-of-mass energies of 16.8, 17.9, and 19.3 MeV, where structure of width $\Gamma = 450 - 750$ keV was observed in the cross section, the angle-averaged alignment is also enhanced relative to nearby energies. We also found that the *angular distributions* of the alignment and differential cross section are remarkably similar to each other at certain energies. This finding is displayed in the form of the angular cross correlation function plotted versus bombarding energy in the top panel of Fig. 5.

Finally, we note that the behavior of the particle-gamma correlation function with respect to particle scattering angle undergoes a striking change as the interaction energy is varied through the region of the narrow resonances. Figure 6 shows $W(\theta)$ for $\psi=90^\circ$, $\phi=40^\circ$, and the lowest 12 energies measured. The periodicity of the correlation function changes abruptly in passing from 17.31 to 17.56 MeV, and again from 18.91 to 19.31 to 19.52 to 20.02 MeV. These features are presumed to reflect interference between the resonances in this energy region and a nonresonant background.

The relative phase angles $\beta=\beta_+-\beta_-$ are presented in Fig. 7. We observe that β generally varies smoothly with angle and energy, and vanishes at $\theta=90^\circ$ as mandated by identical particle symmetry. These findings support the internal consistency of our data. We note, too, that β is better determined in our experiment than is the alignment in that β is independent of the normalization of the correlation function. Other systematics of $\beta(E, \theta)$ are discussed in the next section.

Spin-alignment measurements have also been reported by the Munich group.^{17,18} In that work, gamma radiation was detected at $\psi=0^\circ$ instead of 90° , and thus the measurements could not determine the phase, β . The alignment of the $^{12}\text{C}(2_1^+)$ state was determined in Ref. 18 for four reaction angles ($\theta_{\text{lab}}=19^\circ, 26.5^\circ, 34^\circ,$ and 41.5°) in very small bombarding energy increments over the range $16 \leq E_{\text{c.m.}} \leq 33$ MeV, and results for the two larger angles may be compared with the present data. The comparison can be only approximate, however, since the present data demonstrate a pronounced dependence of alignment on reaction angle (Fig. 3), and the Munich results show that the alignment can change by a factor of 2 when the bombarding energy changes by only 250 keV (c.m.). We interpolated our detailed alignment angular distribution measurements for comparison with the Munich $\theta_{\text{lab}}=34^\circ$ and 41.5° data and found generally good agreement between the results of the two experiments. In particular, at reaction an-

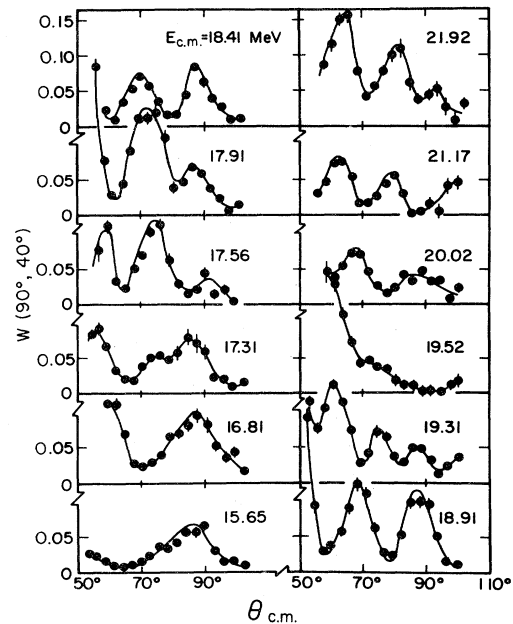


FIG. 6. Variation of the particle-gamma correlation function with energy and reaction angle. For a fixed γ -angle $\psi=90^\circ$ and $\phi=40^\circ$, the correlation function W is plotted versus particle scattering angle for the lowest 12 energies measured. Where no error bars are shown, the statistical errors are smaller than the dots. The lines are drawn only to guide the eye.

gles corresponding to $\theta_{\text{lab}}=41.5^\circ$ (i.e., at $\theta_{\text{c.m.}} \sim 87^\circ-90^\circ$), alignments for 18 of the 21 bombarding energies employed in the present work were consistent with the excitation function of Ref. 18, allowing for the stated uncertainties in the two experiments and for the sharp energy dependence of A . Significant discrepancies appear, however, at $E_{\text{c.m.}}=19.3, 19.5,$ and 20.02 MeV. Our angular distribution measurements reveal deep minima in the

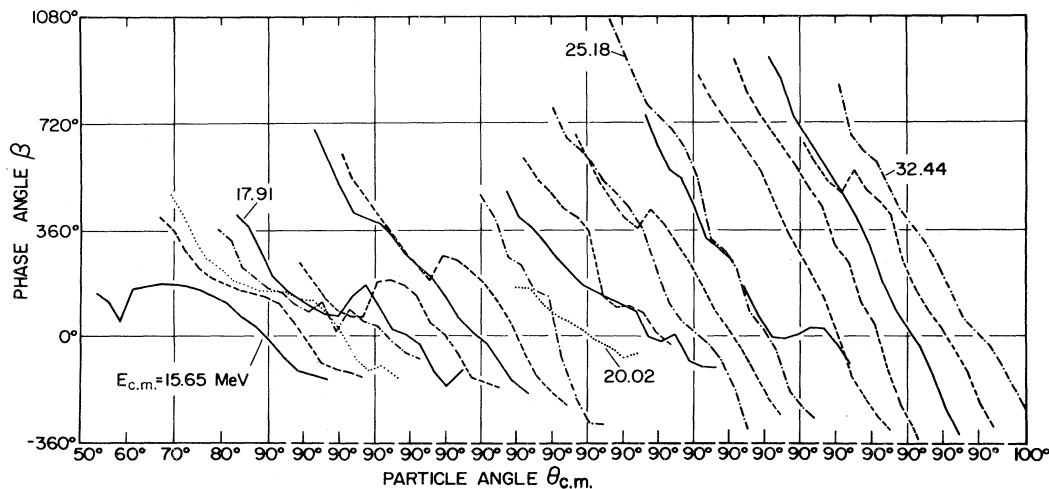


FIG. 7. Phase angle versus particle angle. The angle β from the least squares fit to the correlation function data is plotted versus scattering angle. The different lines (solid, dashed, dotted, and dash-dot) indicate the energies (the same as those listed in Fig. 3) which increase monotonically from left to right in the figure. We observe $\beta(90^\circ)=0$, as expected. Further discussion of the data can be found in the text.

dependence of A on $\theta_{\text{c.m.}}$ near $\theta_{\text{c.m.}} = 90^\circ$ ($\theta_{\text{lab}} = 41.5^\circ$) for the first two of these energies, as may be seen in Fig. 3, and thus the associated discrepancies may result from differences in the actual scattering angles (e.g., different angular resolution, etc., in the two experiments). The comparison at $\theta_{\text{lab}} = 34^\circ$ is similar. Alignments at 16 energies agree within the anticipated uncertainties, while those at five energies ($E_{\text{c.m.}} = 17.91, 21.92, 23.43, 24.43,$ and 25.18 MeV) disagree. The latter four energies are in a region where the Munich excitation function exhibits violent fluctuations, suggesting that these discrepancies may reflect the presence of even more pronounced excitation function structure than was revealed in Ref. 18.

Another experiment employing particle- γ correlations in $^{12}\text{C} + ^{12}\text{C}$ inelastic scattering was recently carried out by the Pennsylvania group.⁷ While the technique was similar and the system identical to ours, the object of their study was different: an exploration of the angular momenta involved in the reaction at energies corresponding to broad maxima in $\sigma(E)$. Hence, the Pennsylvania group performed measurements at many more particle angles, but far fewer energies or gamma angles than we did. There is some overlap in the two sets of data, and in those ranges their correlation functions and ours agree qualitatively (in periodicity and amplitude of the oscillations). A more quantitative comparison is not possible because the data in Ref. 7 are quoted in arbitrary units.

V. DISCUSSION

We have carried out calculations based on previously proposed models of the $^{12}\text{C} + ^{12}\text{C}$ inelastic scattering in order to determine what features are necessary to reproduce all the experimental data now available.

A. Alignment

If we assume equal population of magnetic substates along a quantization axis parallel to the beam, and then rotate those amplitudes for \hat{z} normal to the reaction plane, we obtain $A=0.4$ as the alignment for a random distribution of magnetic substates. However, such a distribution fails to satisfy the consequences of parity conservation embodied in the Bohr theorem, and thus we have adopted $A=0.67$ —reflecting equal population of the $m=-2, 0,$ and $+2$ substates—as a measure of “normal” alignment. Figure 5 illustrates that the measured alignments substantially exceed this value only for bombarding energies where peaks occur in the angle-integrated cross sections, and only for $E_{\text{c.m.}} < 26$ MeV. The simple plane waves approximation, in which only the $m=0$ substate along the recoil direction is populated, yields $A=0.75$ for \hat{z} along $\vec{k}_i \times \vec{k}_f$. This value, which is also independent of energy, applies as a general limit as $\theta \rightarrow 0^\circ$.¹⁴

Other models for the reaction introduce an energy dependence into A . Characteristic features of the alignments predicted with several of these are discussed in subsections 1–5 below. Additional discussion of these matters may be found in the work of Tanimura and Mosel,¹⁴ where the predictions of the strong coupling model (not considered here) are also presented.

1. Single-particle resonances

Cormier *et al.*² interpreted the gross structures in the cross section as resonances, and after postulating spins of $(10^+), (12^+),$ and (14^+) near 13.9, 18.4, and 24.1 MeV, estimated total and partial widths. Treating these as isolated Breit-Wigner resonances, we have attempted to calculate the predicted alignments. In general, the resonant amplitude is added to the background coherently to give a total scattering matrix. Interference between the background and the resonance has an enormous effect on the calculated alignment, and it has been extremely difficult to separate a nonresonant background from the data. In fact, the optical model parameters from elastic scattering⁹ give rise to broad structures in the inelastic scattering similar to those seen in the data. Therefore, this line of analysis is inconclusive.

We can take a different tack and argue that if the broad maxima observed by Cormier and co-workers have a common resonance origin, then other physical observables associated with these structures, such as alignment, might also exhibit common behavior. Yet, as indicated in Fig. 5, while there is broad enhancement in A near 19 and 24 MeV, there is *not* a similar enhancement near 30 MeV. This observation suggests that other explanations for the structure should be pursued.

2. Band crossing model

The band crossing model (BCM) has been successful in reproducing the energies and spins of several Coulomb barrier resonances²⁸ as well as the broader structures in the inelastic and fusion cross sections at higher energies.⁵ We have used these authors' coupled-channel program and the parameters listed in Ref. 5 to calculate the alignment predicted in the higher energy region. A detailed discussion of the BCM alignment predictions has also been given by Tanimura and Mosel.¹⁴ The angle-averaged results from our calculation are compared to the experimental data in Fig. 8.

Unlike Fig. 3 in Ref. 5, Fig. 8(b) addresses the cross section integrated over a limited angular region. While the detailed agreement is not as good as for σ_{tot} , the general features of three broad maxima are still present.

On the other hand, Fig. 8(a) presents a puzzling prediction for the alignment. Over the entire energy range, the calculated alignment is large—a result we expect because the model relies on the crossing of the “aligned inelastic band” with the $n=0$ molecular band^{3,29} to produce resonances. But the relatively small oscillations in the predicted $A(E)$ do not bear any simple relationship to peaks in $\sigma(E)$. This apparent anomaly is cleared up in Fig. 9, which displays the partial cross sections which comprise σ_{tot} and their dominant configurations (aligned or nonaligned). The maxima in the calculated excitation function of $A(E)$ all arise from aligned configurations, but the latter sometimes induce subsidiary shoulders, rather than peaks, in the cross sections. As it turns out, the alignment is a more sensitive measure of the fragmentation of the resonances within this model than is $\sigma(E)$.

It is clear from Fig. 8 that the BCM prediction of alignment does not correspond to the experimental data. The

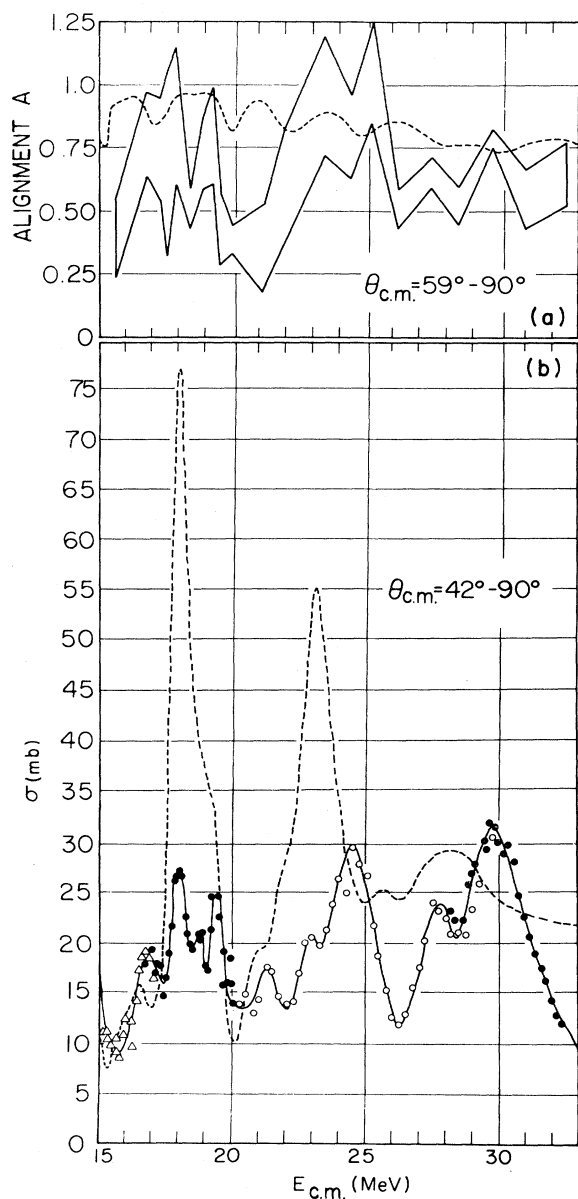


FIG. 8. Band crossing model: alignment and cross section. The solid lines indicate the data, and the dashed lines are BCM calculations (Ref. 5) for $A(E)$ and $\sigma(E)$, each in the angular ranges indicated.

BCM calls for a consistently large alignment, and fails to reproduce the dramatic changes observed in A as the bombarding energy varies.

3. Diffraction model

A simple approach to the scattering of strongly absorbed projectiles was first proposed by Austern and Blair,³⁰ and later extended³¹ and applied to $^{12}\text{C} + ^{12}\text{C}^*$ scattering.⁸ Within this model, broad diffractionlike maxima occur in the cross section excitation function as a consequence of angular momentum and Q -value matching which can be traced to strong absorption and surface tran-

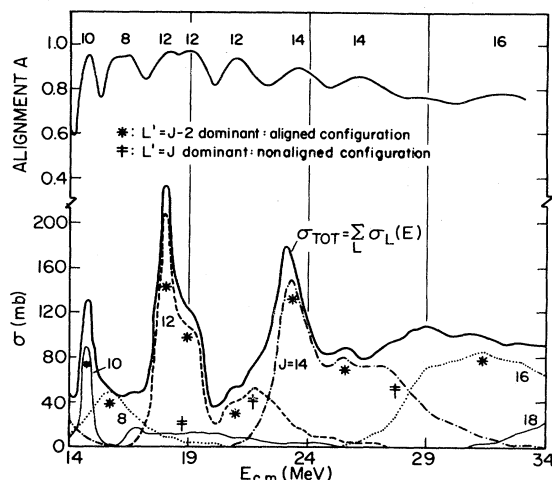


FIG. 9. Band crossing model: partial wave contributions. The numerous oscillations in the predicted $A(E)$ are compared to the partial wave cross sections, denoted by thin solid, dashed, dotted, and dash-dot lines. At energies where the total cross section is dominated by a single component with $L' = J - 2$ (denoted by an asterisk), the alignment reaches a maximum. Energies where $L' = J$ are dominant (crosses) do not have enhanced alignments.

sparency. The diffraction model also predicts enhanced alignment at energies where σ is maximum; moreover, when a single pair of entrance L and exit $L' = L - 2$ orbital angular momenta dominate the reaction, A is predicted to be independent of θ . The latter result is derived in the Appendix.

The predictions and the data for σ and $\langle A \rangle$ are compared in Fig. 10. The gross enhancements in both quantities observed near 18 and 24 MeV are qualitatively reproduced within the model, but the predicted alignments are generally too large. The narrower structures found below 20 MeV are beyond the scope of any single-step non-resonant model. The diffraction model also fails to reproduce the relative constancy of the angle-averaged $A(E)$ above 26 MeV. Finally, the measured angular distributions of the alignment, plotted in Fig. 3, contradict the prediction that A is independent of θ at energies corresponding to gross structure maxima. These results imply a greater participation of several entrance channel partial waves than was assumed in the diffraction model calculations of Phillips *et al.*⁸

Maxima in the cross section arise within the diffraction model from the dominance of a single pair (L, L') of well-matched surface grazing partial waves. In particular, $L' = L - 2$ leads to enhanced alignment. But if the partial wave cutoff were not so sharp, or equivalently, if the optical potential were more diffuse, then several values of L or L' (or both) could contribute at every energy. This situation washes out not only the structure in the predicted cross section, but more especially the structure in the alignment, which depends on the more sensitive requirement that $L' = L - 2$. Analysis of $^{12}\text{C} + ^{12}\text{C}$ elastic and inelastic scattering data taken by Stokstad *et al.*³² at $E = 35 - 63$ MeV indicates that the optical potential ap-

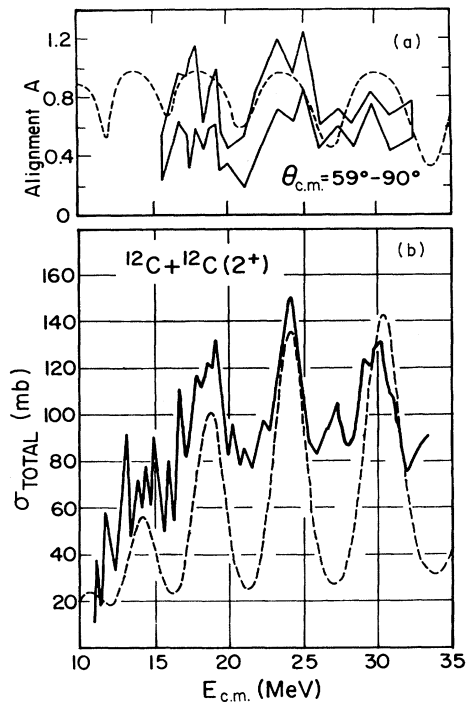


FIG. 10. Diffraction model: alignment and cross section. The solid line in panel (b) is the data from Ref. 2. The dashed lines indicate diffraction model calculations with $\Delta = 1.0$ MeV, as used in Ref. 8. Panel (b) is an integration over $0^\circ - 90^\circ$, while (a) is an average over $59^\circ - 90^\circ$.

appropriate for these higher energies is, indeed, more diffuse. This fact allows several pairs of partial waves to make significant contributions and means that the parametrization of Ref. 8 is definitely not appropriate for higher energy $^{12}\text{C} + ^{12}\text{C}$ scattering. An examination of the inelastic cross section data indicates that the gross structures that dominate the results of Ref. 2 become broader, more widely spaced, and less prominent above 32 MeV in Ref. 32. These results, together with the present data, indicate the onset of a transition region near $E_{c.m.} = 26 - 30$ MeV between two distinct behaviors. Below 26 MeV, strong alignment is indeed observed at certain (resonance) energies, but the extreme alignment corresponding to the dominance of a single pair (L, L') of partial waves with $L' = L - 2$ is not a general feature of the data. Additional discussion of the alignment predicted by the diffraction model may be found in Ref. 14.

4. DWBA

Cannell *et al.*⁷ have demonstrated that distorted-wave Born approximation (DWBA) calculations, using parameters from the optical model determined by Reilly *et al.*⁹ but with the radii decreased by 4.75%, can reproduce the broad features observed in the $^{12}\text{C} + ^{12}\text{C}$ inelastic scattering between 15 and 32 MeV.

We have modified the computer code DWUCK (Ref. 33) to account for identical particle symmetry, and calculated m -substate population parameters using the optical model

parameters employed in Ref. 7. The results, averaged over the same angular range as the data, are graphed in Fig. 11. While the DWBA predicts broad oscillations in A as well as in σ , the maxima in A occur approximately 1 MeV higher in energy, in contrast to the measured behavior. Furthermore, the small amplitude oscillations in the predicted alignment (arising from the model parameters, and not from the angle averaging) are far too gentle to reproduce the trend of the experimental data. While this comparison with the data does not rule out the DWBA approach in general, it does at least indicate that different parameters are needed to simultaneously reproduce the elastic, inelastic, and alignment data.

5. Barrier top model

Structure arises within the diffraction model from energy-angular momentum windows for inelastic scattering; these windows move up in L space as the beam energy is increased. Friedman *et al.*¹¹ point out that such a condition is consistent with the occurrence of orbiting-type "barrier top resonances,"³⁴ which exist when strong inter-

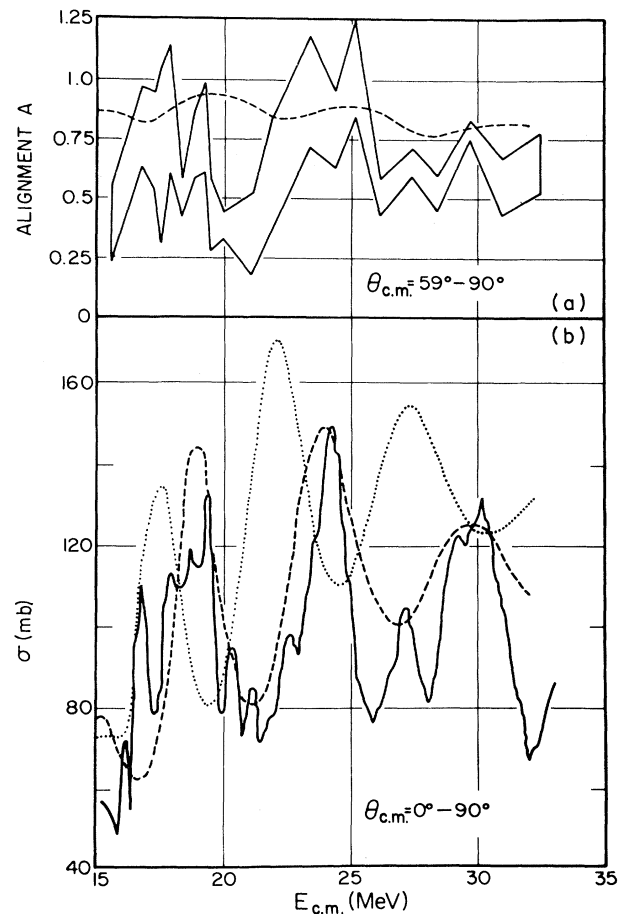


FIG. 11. DWBA: alignment and cross section. The data indicated by the solid lines are the same as in Fig. 10. The dotted line is the prediction of the DWBA using the optical model parameters of Ref. 9. Adjustment of the well radii, as in Ref. 7, yields the dashed-line predictions.

nal absorption makes classical potential “pocket” resonances untenable. There has been some difficulty in sorting out the differences between the diffraction and the barrier top models. Each interpretation arises from the same physical situation—strong internal absorption and surface transparency in the one-channel optical potentials—and each relies on energy-angular momentum windows to generate gross structures in the cross section.

We have explored the extent to which the characteristic predictions of the barrier-top and diffraction models depend on the particular forms chosen for the parametrization of the participating angular momenta. The barrier top model uses a width parameter, Γ_L , which, as the beam energy is increased, guarantees a constant width of the resonances in L space and a rapidly increasing energy width. On the other hand, the diffraction model, as implemented in Ref. 8, employs Δ , a constant energy width which leads to decreasing L width for higher incident energies. Taken alone, the barrier top model cannot predict either differential cross sections or alignments because the phases of the radial integrals are not specified.³⁵ We have, however, performed some hybrid calculations to study the relation between the diffraction and the barrier top models. First, we tried to parametrize the S matrix not in E space,⁸ but in L space³⁴:

$$\eta_L = (1 - \exp\{2\pi[L - L_{\text{orb}}(E)]/\Gamma_L\})^{-1/2}. \quad (8)$$

Again, we used the Austern-Blair-Hahne relation to obtain the radial integrals, and we obtained cross sections quite similar to those reported in Ref. 8 and alignments very close to those in Fig. 10. Apparently, the diffraction model is not sensitive to the particular method of parametrizing the S matrix over this restricted energy range, provided appropriate values are chosen for the parameters.

Second, we replaced the radial integral in the diffraction calculation by the two-pole prescription of Friedman *et al.*¹¹ The resulting angle-integrated cross sections were similar to those published in Ref. 11, but the predicted angle-averaged alignments decreased smoothly with energy, showing *no* gross structure. However, the lack of phase specification within the barrier top model may well be crucial, and an additional ansatz concerning the phase may be necessary to reproduce the alignment data.

B. Phase angle

As demonstrated in the Appendix, the application of the high angular momentum limit simplifies analytical expressions for the correlation and produces easily-tested relations. In particular, the further assumption of $L' = L - 2$ leads to a predicted linear behavior of $\beta(\theta)$, with a slope equal to $-(2L' + 1)$.

With the same amplitudes that were used to obtain alignment predictions, we calculated the phase angles expected within the band crossing, diffraction, and DWBA models. For all energies considered, the band crossing and diffraction models each predict β to be linear in θ , as expected from the treatment in the Appendix. Near energies where maxima occur in $\sigma(E)$ (18, 24, and 30 MeV), the slope calculated within each model is very close to

$-(2L' + 1)$. This agreement once again confirms the dominance of the aligned configuration ($L' = L - 2$) in the band crossing and diffraction models at those energies. The energy dependence of β for energies between these plateaus (near 15, 21, and 27 MeV) is slightly different for the two types of calculations. Yet, it is revealing that these two models—one involving coupled channels and based on the existence of resonances, the other a one-step process with no resonances—give predictions for β that are practically identical.

A DWBA treatment, as applied by Cannell and collaborators,⁷ yields a somewhat different behavior of the phase angle, as shown in Fig. 12 together with the data. For $E = 18$ –21, 23–26, and 28–33 MeV, the DWBA predicts $\beta(\theta)$ to be very similar to the BCM or diffraction model results, with only gentle oscillations about a straight-line trend. But for the other energies calculated, the DWBA phase angle deviates from monotonic behavior at the more forward angles, and for some energies (17–18 and 22 MeV) exhibits cusps. At one energy, 17.91 MeV, such behavior also appears in the data.

The correspondence of the model calculations to each other and to experiment varies with energy. Near 18, 24, and 30 MeV, where gross structure appears in the cross section data, all models successfully reproduce the observed linear dependence of the phase angle on reaction angle. Approximately 1 MeV above those energies, the measured and calculated phases agree for $\theta > 70^\circ$, but are 180° out of phase forward of that angle. Near 21 and 26 MeV the predictions become completely out of phase with the data at all angles. The physics underlying these phenomena is not understood. It would appear, however, that contributions from nonaligned configurations are significantly larger than predicted by the diffraction and band crossing models, especially for energies between gross structure maxima. Similar conclusions have been drawn by Balamuth *et al.*⁷ and by Tanimura and Mosel.¹⁴ The phase data near $E_{\text{c.m.}} = 18, 24, \text{ and } 30$ MeV support an interpretation in terms of strongly aligned configurations for these energies, but this is contradicted at $E_{\text{c.m.}} = 30$ MeV by the magnitude of the observed angle-averaged alignment. Further theoretical work will be required to exploit the phase information from the present experiment in an effort to delineate the details of the $^{12}\text{C} + ^{12}\text{C}$ reaction mechanism(s).

We also note in connection with Fig. 12 that the apparent slopes of $\beta(\theta)$ over all or part of the angular range measured are much smaller than predicted by the models for $E = 16$ –17.8 and 19.5–20 MeV. This behavior might be related to the narrow resonances observed in other exit channels of the $^{12}\text{C} + ^{12}\text{C}$ reaction near this energy. Again, further theoretical analysis needs to be done to establish whether $\beta(\theta, E)$ contains information concerning the resonances.

VI. CONCLUSIONS

Faced with a number of models put forth to explain structures observed in the cross section for $^{12}\text{C} + ^{12}\text{C}(2^+)$ scattering at higher energies, we have undertaken to measure additional physical observables of the reaction. Using a particle-gamma correlation technique, we obtained

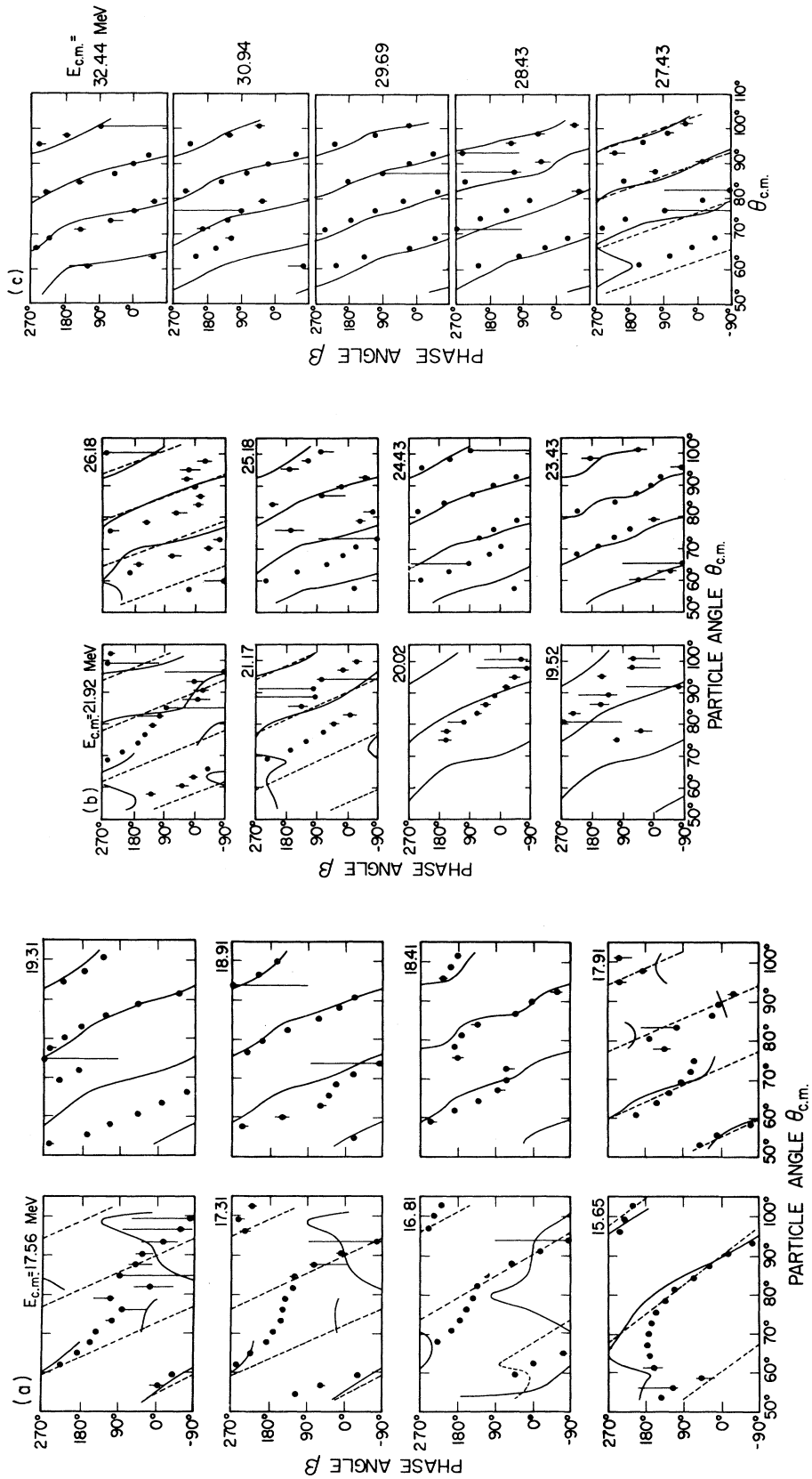


FIG. 12. Phase angles versus particle scattering angles. The solid dots and error bars are the experimental data. The solid lines are the DWBA predictions using the parameters of Ref. 7. At energies where the diffraction and band crossing model predictions (which are practically identical) differ substantially from the DWBA, the BCM values are shown as dashed lines. Some of the error bars seem skewed because the formalism actually derives $\tan\beta$, and not β , from the least squares parameters [see Eq. (7)].

the alignments and the relative substate phases for a wide range of particle angles, and for energies that map over both the broad and narrow structures in $\sigma(E)$.

The measured alignment depends strongly on reaction angle and bombarding energy and, as a consequence, conclusions based on measurements at isolated angles or energies may be misleading. In general, the alignment averaged over the reaction angles is strongly (and positively) correlated with both the broad and narrow structures observed in the total inelastic cross section for $E < 26$ MeV. Above that energy, the average alignment is less sensitive to variations in bombarding energy, and it oscillates within a narrow band about the "normal" value of $A=0.67$, indicative of a change in the characteristic features of the $^{12}\text{C} + ^{12}\text{C}$ interaction.

Neither the band crossing model nor the DWBA is successful in describing the gross structure observed in the excitation function for the angle-averaged alignment. The former model predicts too many peaks at the wrong energies and with peak-to-valley ratios that are too small. The latter calculations exhibit too little structure in $A(E)$, with peaks incorrectly placed. The diffraction model is somewhat more successful in that prominent peaks in $A(E)$ are predicted at the appropriate energies, but as is the case with all the models considered, it tends to overestimate the degree of alignment at all energies. Thus, none of the models provide an adequate description of the angle-averaged alignment.

The angular distributions of the alignment and of the relative phase between the $m = \pm 2$ wave functions contain detailed information concerning the reaction mechanism. These quantities are poorly described, in general, by the models considered. The behavior of the angular distributions indicates that for most energies several partial waves contribute strongly to the inelastic excitation process, in contradiction to the assumptions of current models. However, the observed linear dependence of the relative phase on reaction angle at energies corresponding to gross structure maxima in the cross section near $E_{c.m.} \sim 18$ and 24 MeV is characteristic of strong alignment and the dominance of a single pair of partial waves with $L'=L-2$.

The narrow structures below 20 MeV, whose width and correlations with other exit channels indicate a genuine resonance origin, are characterized in our work by

$$\sqrt{\sin\theta}\Psi \propto \sum_m \left[\sum_{\mu} \langle L' - \mu 2\mu | LO \rangle \sqrt{\sin\theta} Y_{L'}^{-\mu}(\theta, \phi) D_{\mu m}^2(R) \right] \chi_2^m. \quad (\text{A3})$$

The quantity in brackets is $a_m = \alpha_m e^{i\beta} m$, the complex amplitude to populate substate m with any chosen quantization axis. We want $\hat{z} = \hat{k} \times \hat{k}'$ perpendicular to the reaction plane, and we make the arbitrary choice $\hat{y} = \hat{k}'$, which later leads to a_m independent of ϕ . The Euler angles effecting this transformation are $\alpha = -\phi + \pi/2$, $\beta = -\pi/2$, and $\gamma = 0$, and the rotation matrix is

$$D_{\mu m}^2(R) = e^{i\mu\phi - i\mu\pi/2} d_{\mu m}^2 \left[-\frac{\pi}{2} \right]. \quad (\text{A4})$$

enhanced alignment, unusually small slopes in $\beta(\theta)$, and a striking change in the pattern of the correlation function $W(\theta)$.

ACKNOWLEDGMENTS

We thank Dr. Y. Kondo for the use of his BCM computer code and for helpful discussions. The material in the Appendix is based on correspondence from Dr. J. Wenener, for which we are grateful. One of us (K.A.E.) wishes to thank Dr. G. R. Satchler for many valuable discussions concerning angular correlations, and Dr. J. Beene for advice concerning relativistic corrections to the measured correlation function. This work was supported by U. S. Department of Energy under Contract No. EY-76-C-02-3074 with Yale University, and Contract No. W-7405-eng-26 with Union Carbide Corporation.

APPENDIX

Using the limit of high orbital angular momentum and the simplifying assumption of $L'=L-2$, the angular dependence of A and β can be derived analytically.³⁶

We start with an expression for the angular dependence of the wave function $\Psi(\theta, \phi)$:

$$\sqrt{\sin\theta}\Psi \propto \sum_{\mu} \langle L' - \mu 2\mu | LO \rangle \sqrt{\sin\theta} Y_{L'}^{-\mu}(\theta, \phi) \chi_2^{\mu}. \quad (\text{A1})$$

Here, we have dropped nonessential constants and multiplied by the factor $\sqrt{\sin\theta}$ that would normally be introduced into an integration over solid angle, so that all angle-dependent terms are included. We sum over the magnetic substates μ of the $I=2$ state excited in the scattering; χ_2^{μ} is the spin wave function for that substate. L and L' are the incoming and outgoing orbital angular momenta, respectively. (A1) is the standard expression obtained by defining the beam axis \hat{k} as the quantization axis \hat{z} . A rotation of the coordinate axes introduces different spin wave functions:

$$\chi_2^{\mu} = \sum_m D_{\mu m}^2(R) \chi_2^m. \quad (\text{A2})$$

Inserting (A2) into (A1) yields:

The spherical harmonics are written in terms of associated Legendre polynomials, and we take the asymptotic value of the latter in the limit of large angular momentum l to obtain:

$$Y_l^m(\theta, \phi) \approx (-)^m \left[\frac{2l+1}{8 \sin\theta} \frac{(l-m)!}{(l+m)!} \right]^{1/2} \frac{\Gamma(l+m+1)}{\Gamma(l+3/2)} \times \cos \left[\left(l + \frac{1}{2} \right) \theta - \frac{\pi}{4} + \frac{m\pi}{2} \right] e^{im\phi}. \quad (\text{A5})$$

For our case $l=L' \geq 10$, which is sufficiently large to make this limit valid for θ not close to 0 or 180° . Also, $l \gg m$, and we drop factors in (A5) that are constant in this approximation. Insertion of (A4) and (A5) into (A3) then gives

$$a_m = \sum_{\mu} \langle L' - \mu 2\mu | LO \rangle \cos(\omega - \frac{1}{2}\mu\pi) \times e^{-i\mu\pi/2} d_{\mu m}^2 \left[-\frac{\pi}{2} \right]. \quad (\text{A6})$$

Here we have defined ω as $(L' + \frac{1}{2})\theta - \pi/4$. Making the further assumption $L' = L - 2$ leads us to the evaluation of the Clebsch-Gordan coefficients:

$$\begin{aligned} \langle L' - \mu 2\mu LO \rangle &= \left[\frac{L'(L' - 1)}{16(L' + \frac{1}{2})(L' + \frac{3}{2})} \right]^{1/2} \approx \frac{1}{4} \\ &\quad \text{for } \mu = \pm 2, \\ &= \left[\frac{L'(L' + 2)}{4(L' + \frac{1}{2})(L' + \frac{3}{2})} \right]^{1/2} \approx \frac{1}{2} \\ &\quad \text{for } \mu = \pm 1, \\ &= \left[\frac{3(L' + 1)(L' + 2)}{8(L' + \frac{1}{2})(L' + \frac{3}{2})} \right]^{1/2} \approx \sqrt{3/8} \\ &\quad \text{for } \mu = 0. \quad (\text{A7}) \end{aligned}$$

The expressions (A7) are used to evaluate the sum in (A6), leading to the results

$$a_m = \frac{1}{2}(\cos\omega \mp i \sin\omega) \quad \text{for } m = \pm 2 \\ = 0 \quad \text{for } m = 0, \pm 1. \quad (\text{A8})$$

Hence, $\alpha_+^2 = \alpha_-^2$, independent of ω , while $\alpha_0^2 = 0$. With the approximations $L' = L - 2$ and L' large, alignment is complete ($A = 1$) and independent of the particle scattering angle. A variation of alignment with angle would indicate a significant admixture of the $L = L'$ component of the scattering.

The phase angle from (A8) is

$$\beta = \beta_+ - \beta_- = -2\omega = -\frac{\pi}{2} - (2L' + 1)\theta. \quad (\text{A9})$$

Linear behavior of $\beta(\theta)$ with slope $-(2L' + 1)$ would most probably reflect dominance of $L' = L - 2$ in the scattering, although a combination of (L, L') values at a given energy might conspire to give a linear character to $\beta(\theta)$ with an apparently anomalous slope.

*Present address: 3M Company, St. Paul, MN 55144.

†Present address: Bell Laboratories, Holmdel, NJ 07733.

‡Present address: Canberra Industries, Meriden, CT 06450.

§Permanent address: Oak Ridge National Laboratory, Oak Ridge, TN 37830.

¹T. M. Cormier, J. Applegate, G. M. Berkowitz, P. Braun-Munzinger, P. M. Cormier, J. W. Harris, C. M. Jachcinski, L. L. Lee, Jr., J. Barrette, and H. E. Wegner, Phys. Rev. Lett. **38**, 940 (1977).

²T. M. Cormier, C. M. Jachcinski, G. M. Berkowitz, P. Braun-Munzinger, P. M. Cormier, M. Gai, J. W. Harris, J. Barrette, and H. E. Wegner, Phys. Rev. Lett. **40**, 924 (1978).

³W. Scheid, W. Greiner, and R. Lemmer, Phys. Rev. Lett. **25**, 176 (1970); H.-J. Fink, W. Scheid, and W. Greiner, Nucl. Phys. **A188**, 259 (1972); J. Y. Park, W. Scheid, and W. Greiner, Phys. Rev. C **10**, 967 (1974).

⁴R. Koennecke, W. Greiner, J. Y. Park, and W. Scheid, in *Resonant Behavior of Heavy Ion Systems*, edited by G. Vourvopoulos (National Printing Office, Athens, 1981), p. 163, and references therein.

⁵Y. Kondo, Y. Abe, and T. Matsuse, Phys. Rev. C **19**, 1356 (1979).

⁶O. Tanimura, Nucl. Phys. **A334**, 177 (1980).

⁷L. E. Cannell, R. W. Zurmühle, and D. P. Balamuth, Phys. Rev. Lett. **43**, 837 (1979); D. P. Balamuth, L. E. Cannell, and R. W. Zurmühle, Phys. Rev. C **23**, 2492 (1981).

⁸R. L. Phillips, K. A. Erb, D. A. Bromley, and J. Weneser, Phys. Rev. Lett. **42**, 566 (1979).

⁹W. Reilly, R. Wieland, A. Gobbi, M. W. Sachs, and D. A.

Bromley, Nuovo Cimento **13A**, 897 (1973).

¹⁰S. Y. Lee, Y. H. Chu, and T. T. S. Kuo, Phys. Rev. C **24**, 1502 (1981).

¹¹W. A. Friedman, K. W. McVoy, and M. C. Nemes, Phys. Lett. **87B**, 179 (1979).

¹²P. Paul, in *Resonances in Heavy Ion Reactions*, edited by K.A. Eberhard (Springer, New York, 1982), p. 161.

¹³O. Tanimura and U. Mosel, Phys. Rev. C **24**, 321 (1981).

¹⁴O. Tanimura and U. Mosel, Phys. Lett. **114B**, 7 (1982).

¹⁵S. J. Willett, K. A. Erb, S. K. Korotky, R. L. Phillips, and D. A. Bromley, in Proceedings of the International Conference on Nuclear Physics, edited by R. M. Diamond and J. O. Rasmussen, Lawrence Berkeley Laboratory Report LBL-11118, 1980, Vol. 1, p. 550.

¹⁶K. A. Erb, in *Resonant Behavior of Heavy Ion Systems*, edited by G. Vourvopoulos (National Printing Office, Athens, 1981), p. 321.

¹⁷W. Trombik, W. Dunnweber, W. Trautmann, W. Dahme, K. A. Eberhard, W. Hering, D. Konnerth, and R. Singh, Z. Phys. A **296**, 187 (1980).

¹⁸W. Trombik, in *Resonances in Heavy Ion Reactions*, edited by K. A. Eberhard (Springer, New York, 1982), p. 297.

¹⁹T. D. Hayward and F. H. Schmidt, Phys. Rev. C **1**, 923 (1970).

²⁰A. Bohr, Nucl. Phys. **10**, 486 (1959).

²¹See, e.g., S. J. Willett, Ph.D. thesis, Yale University, 1981 (unpublished).

²²D. R. James and N. R. Fletcher, Phys. Rev. C **17**, 2248 (1978).

²³K. Van Bibber, E. R. Cosman, A. Sperduto, T. M. Cormier, T.

- N. Chin, and O. Hansen, Phys. Rev. Lett. 32, 687 (1974).
- ²⁴P. Sperr, D. Evers, K. Rudolph, W. Assmann, E. Spindler, P. Konrad, and G. Denhofer, Phys. Lett. 49B, 345 (1974).
- ²⁵G. Kekelis and J. D. Fox, Phys. Rev. C 10, 2613 (1974).
- ²⁶E. R. Cosman, R. Ledoux, M. J. Bechara, C. Ordonez, R. Valicenti, and A. Sperduto, MIT report 1981 (unpublished). See also Ref. 27.
- ²⁷E. R. Cosman, R. J. Ledoux, M. J. Bechera, C. E. Ordonez, and H. A. Al-Juwair, in *Resonances in Heavy Ion Reactions*, edited by K. A. Eberhard (Springer, New York, 1982), p. 123.
- ²⁸Y. Kondo, T. Matsuse, and Y. Abe, Contributed paper VIIB.5 to 2nd International Conference on Clustering Phenomena in Nuclei, edited by D. A. Goldberg, J. B. Marion, and S. J. Wallace, University of Maryland report, 1975.
- ²⁹A. Arima, G. Scharff-Goldhaber, and K. W. McVoy, Phys. Lett. 40B, 7 (1972).
- ³⁰N. Austern and J. S. Blair, Ann. Phys. (N.Y.) 33, 15 (1965).
- ³¹F. J. W. Hahne, Nucl. Phys. A104, 545 (1967).
- ³²R. G. Stokstad, R. M. Wieland, G. R. Satchler, C. B. Fulmer, D. C. Hensley, S. Raman, L. D. Rickertsen, A. H. Snell, and P. H. Stelson, Phys. Rev. C 20, 655 (1979).
- ³³P. D. Kunz, DWUCK, University of Colorado computer code (unpublished).
- ³⁴W. A. Friedman and C. J. Goebel, Ann. Phys. (N.Y.) 104, 145 (1977).
- ³⁵W. A. Friedman, private communication.
- ³⁶J. Weneser, private communication.